Ionization and radiation dynamics of dense MHD plasmas[a)]

Dwight Duston[b)]

Department of Physics, The University of Michigan, Ann Arbor, Michigan 48109

James J. Duderstadt

Department of Nuclear Engineering, The University of Michigan, Ann Arbor, Michigan 48109
(Received 11 July 1977; accepted for publication 1 November 1977)

The ionization and radiation dynamics of dense magnetohydrodynamic plasmas has been modeled in a fashion suitable for implementation in MHD computer simulation codes. It has been shown that more restrictive LTE models such as those based on the Saha equation are inadequate to describe the rapidly varying temperature and density regimes characterizing many such plasmas. Detailed collisional-radiative models are developed which directly solve the time-dependent rate equations characterizing atomic processes along with those equations characterizing the hydrodynamic motion of the plasma. These models are applied to analyze high-density-helium Z-pinch and lithium exploding-wire plasmas, and they are found to yield results which compare quite favorably with experimental data.

PACS numbers: 52.65.+z, 52.25.Ps, 52.55.Ez, 52.50.Lp

I. INTRODUCTION

An accurate theoretical description of the ionization state and excited-level populations of a dense dynamic plasma is necessary for the development of suitable diagnostics and interpretation of data obtained for a variety of experimental plasma studies. In the past, most models of the plasma atomic state have been based upon equilibrium or quasi-equilibrium assumptions. In this work, we will examine the suitability of several of these models for incorporation into a magnetohydrodynamic description of dense pinch plasmas. We will first compare the results and validity of a Saha model (based on the assumption of local thermodynamic equilibrium[1] in the plasma) with a rate-equation calculation [based on a collisional-radiative (CR) model[2]] for dense plasmas. Particular attention will be directed towards the theoretical study of an ultrahigh-density-helium Z-pinch and a lithium exploding-wire experiment which are analyzed by coupling the ionization model and radiation dynamics into a standard MHD simulation code. Comparison of these results with experimental measurements taken in our plasma laboratory will also be presented.

II. MODELS OF THE IONIZATION DYNAMICS OF PLASMAS

A. Local thermodynamic equilibrium (LTE) models

The assumption that a plasma can be adequately characterized by an LTE state allows the use of the Saha equation for calculating the various ion-state population densities. Since this is an equilibrium model, it is only implicitly time dependent (through the time variation of the state variables) and relies solely on the statistical law of energy equipartition and not on any specific knowledge of atomic collisional cross sections. That is, while this model allows for the variation of the local temperature, density, and chemical composition of the plasma, it assumes that the ion-density populations depend only on these thermodynamic quantities and not explicitly upon time.

The equations for LTE plasmas depend on the detailed balancing of the dominant *collisional* processes in the plasma: collisional (three body) recombination and collisional (two-body) ionization between ion species, and collisional excitation and deexcitation between levels within a single species. Using equations for these processes given by Seaton[3] and Griem,[4] we can write a generalized Saha-Boltzmann equation in the form

$$\frac{n(z+1)n_e}{n(z,j)} = \frac{2U(z+1)}{U(z)}\left(\frac{2\pi m_e k_B T_e}{h^2}\right)^{3/2} \times \exp\left(\frac{\chi(z,j)-\Delta E(z)}{k_B T_e}\right) \text{ cm}^{-3}, \quad (1)$$

where $n(z,j)$ is the ion population of charge state z in excited level j, n_e is the electron density, U is the partition function, m_e is the electron mass, T_e is the electron temperature, k_B is Boltzmann's constant, $\chi(z,j)$ is the ionization potential of level j, and ΔE is the ionization reduction. The latter term is defined by Griem[4] as

$$\Delta E(z) = \frac{Ze^2}{4\pi\epsilon_0 \rho_D}, \quad (2)$$

where ρ_D is the Debye radius,

$$\rho_D = \left(\frac{\epsilon_0 k_B T_e}{e^2[n_e + \Sigma_z Z^2 n_i(z,0)]}\right)^{1/2} \text{ cm}, \quad (3)$$

where e is the electron charge and ϵ_0 is the permittivity of vacuum. The partition function $U(z)$ is defined as

$$U(z) \cong \tfrac{2}{3}(2S_1+1)(2L_1+1)\left(\frac{Z^2 E_H}{\Delta E(z)}\right)^{3/2} \times \exp\left(\frac{\chi(z,j)-\Delta E(z)}{k_B T_e}\right) + \sum_j^j g(z,j)\exp\left(-\frac{E(z,j)}{k_B T_e}\right), \quad (4)$$

a)Work supported by the Air Force Office of Scientific Research.
b)Permanent address: Naval Research Laboratory, Washington, D.C. 20375.

 0021-8979/78/4908-4388$01.10

where S_1 and L_1 are the spin angular momentum and orbital angular momentum of the ground state of the $z+1$ ion and E_H is the ionization potential of hydrogen. The sum is performed to the highest level j' below the reduced ionization limit $\chi(z,0)-\Delta E(z)$, but in our model, the sum was truncated at the fourteenth excited level of the ion species. This model was used in calculating the ground states of the plasmas only, and it was employed in the description of both helium and lithium plasmas.

The particular model for helium includes three equations of the form in Eq. (1), one each for the ground states of He I, He II, and He III, while the lithium model includes an additional equation for Li IV. These Saha equations are solved simultaneously with an equation expressing plasma neutrality,

$$n_e=\sum_z zn(z,0), \tag{5}$$

where the sum is taken over all charge states of the atom.

B. Collisional-radiative (CR) model

A more sophisticated model which takes into account nonequilibrium, collisional, and radiative processes was also applied to analyze dense helium and lithium plasmas. This model directly solves the rate equations describing the various atomic processes occurring in the plasma:

(i) collisional ionization

$n(z,j)+e^-\rightarrow n(z+1,0)+e^-+e^-$,

(ii) collisional (three-body) recombination

$n(z,0)+e^-+e^-\rightarrow n(z-1,j)+e^-$,

(iii) radiative (two-body) recombination

$n(z,0)+e^-\rightarrow n(z-1,j)+h\nu$,

(iv) spontaneous emission (radiative decay)

$n(z,i)\rightarrow n(z,j)+h\nu$,

(v) collisional excitation

$n(z,j)+e^-\rightarrow n(z,i)+e^-$,

(vi) collisional deexcitation

$n(z,i)+e^-\rightarrow n(z,j)+e^-$.

It should be noted that the processes of photoionization, excitation, and deexcitation have been ignored, limiting the validity of this CR model to plasmas of sufficient optical thinness that these processes are negligible. In addition, we have chosen not to include the process of dielectronic recombination in our rate equations. Although this process is a major contributor to the total line emission in higher-Z plasmas,[5] it is believed to have a negligible effect on both the radiation energy balance and the excited-state population densities of the low-Z plasmas considered in this work.

Including only the processes described above, the CR model equations[6] can be written as

$$\begin{aligned}\frac{dn(z,j)}{dt}=&\Big(n_e n(z-1,j'')S(z-1,j'';z,j)+n_e n(z+1,j')\\&\times[\alpha(z+1,j';z,j)+n_e\beta(z+1,j';z,j)]\\&+\sum_{i>j}n(z,i)A(i,j)+n_e\sum_{i>j}n(z,i)X^{-1}(i,j)\\&+n_e\sum_{i<j}n(z,i)X(i,j)\Big)-n(z,j)\Big(n_eS(z,j;z+1,j')\\&+n_e[\alpha(z,j;z-1,j'')+n_e\beta(z,j;z-1,j'')]\\&+\sum_{i<j}A(j,i)+n_e\sum_{i<j}X^{-1}(j,i)+n_e\sum_{i>j}X(j,i)\Big),\end{aligned} \tag{6}$$

where $n(z,j)$ is the population density of ion species z in level j, $S(z-1,j'';z,j)$ is the collisional ionization rate (cm^3/sec) from $n(z-1,j'')$ to $n(z,j)$, α is the radiative recombination rate (cm^3/sec), β is the collisional recombination rate (cm^6/sec), $A(i,j)$ is the spontaneous decay rate from levels i to j (1/sec), $X(i,j)$ is the collisional excitation rate from i to j (cm^3/sec), and $X^{-1}(i,j)$ is the inverse reaction collisional deexcitation. The terms in the first set of large parentheses on the right-hand side of Eq. (6) express the increase in population density of $n(z,j)$ from surrounding states, while the terms in the second set of large parentheses give the rate of loss from $n(z,j)$. If we eliminate the terms describing excitation and deexcitation, then Eq. (6) describes a model of ground states only. This ground-state model was used for both helium and lithium plasma simulations in a quasiequilibrium mode, i.e., neglecting the time derivative on the left-hand side.

Since the energy deposition in these plasmas occurs on a time scale long compared to that of atomic processes, and, often, no detailed information of the excited levels or line emission was required, this shorter version of the model was very useful. In addition, a version was also used for lithium which included several excited states, as shown in Fig. 1, and explicitly accounted for the time rate of change of the ion-state densities.

The accuracy of the CR model in predicting the actual plasma state will depend primarily on how well the rate coefficients reflect the reaction cross sections in the various temperature and density regimes during the plasma time evolution. The rates used in this study are similar to those used in Davis and Whitney's[7] work on higher-Z materials. The ionization-rate coefficient was obtained from Seaton's[3,8] result after integrating over a Maxwellian velocity distribution,

$$S(z,j;z+1,0)=2.429\times10^{-6}\frac{\xi_z T_e^{1/2}}{\chi(z,j)^2}\exp\left(\frac{-\chi(z,j)}{T_e}\right)\frac{\text{cm}^3}{\text{sec}} \tag{7}$$

(T_e and χ in eV), where ξ is the number of outer shell electrons. The radiative recombination rate is given by Seaton,[9] and while it is derived for hydrogenic ions, it is used for all ion species due to lack of a better expression,

$$\begin{aligned}&\alpha(z,0;z-1,j)\\&\quad=5.2\times10^{-14}Z\phi^{1/2}(0.43+\tfrac{1}{2}\ln\phi+0.47\phi^{-1/3})\ \text{cm}^3/\text{sec},\end{aligned} \tag{8}$$

where Z is the ion charge and $\phi=\chi(z-1,j)/T_e$. The collisional recombination rate can be calculated by using the principle of detailed balance between ionization and recom-

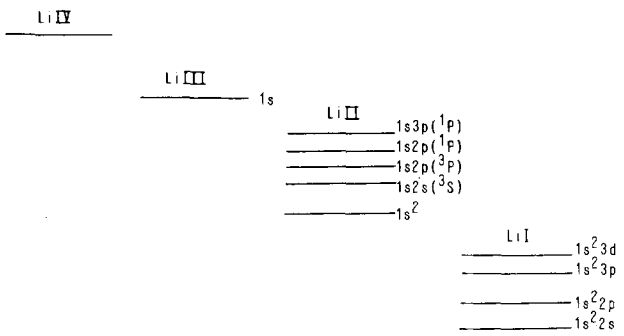

FIG. 1. Atomic states included in the rate-equation model for lithium.

bination due to electron collisions to find

$$\beta(z,0;z-1,j) = 8.051\times10^{-28}\frac{\xi_z g(z-1,j)}{2g(z,0)}\frac{1}{\chi(z-1,j)^2 T_e}\frac{\text{cm}^6}{\text{sec}}. \quad (9)$$

The coefficient for spontaneous emission is just the Einstein coefficient and the values were taken from the NBS tables.[10] The rate coefficients for collisional excitation and deexcitation were calculated using the semiclassical impact parameter (SCI) method of Burgess[11] and can be expressed in terms of the oscillator strength f_{ij},

$$X(i,j) = 1.578\times10^{-5}\frac{f_{ij}\langle\bar{g}_{ij}\rangle}{E_{ij}T_e^{1/2}}\exp\left(-\frac{E_{ij}}{T_e}\right)\frac{\text{cm}^3}{\text{sec}}, \quad (10)$$

where $\langle\bar{g}_{ij}\rangle$ is a thermally averaged Gaunt factor and E_{ij} is the term energy in eV. The deexcitation rates are given by detailed balance with the excitation rate,

$$X^{-1}(j,i) = X(i,j)\frac{g(z,i)}{g(z,j)}\exp\left(\frac{E_{ij}}{T_e}\right)\frac{\text{cm}^3}{\text{sec}}. \quad (11)$$

The value of the Gaunt factor g_{ij} was given as the threshold value of 0.2 by Seaton,[7] but Allen[12] later recalculated it to give higher values at higher energies. However, these universal values were shown to be incorrect for many transitions (particularly, resonance transitions) by Oran and Davis.[13] Their expression for the thermally averaged Gaunt factor is

$$\langle\bar{g}_{ij}\rangle = \left[\int_E^\infty \bar{g}_{ij}\exp(-E/T_e)\,dE\right] \times\left[\int_E^\infty \exp(-E/T_e\,dE)\right]^{-1}, \quad (12)$$

but a simple analytic expression fitted to their curves is given by Davis,[14]

$$\langle\bar{g}_{ij}\rangle = A+(BY+C)\left[\ln\left(\frac{Y+1}{Y}\right)-\frac{0.4}{(Y+1)^2}\right], \quad (13)$$

where A, B, and C are constants dependent on the transition and $Y=E_{ij}/T_e$.

The excited states used in the lithium model were chosen so as to calculate line ratios which could be compared to experimental measurements. Higher-level states were neglected due to computer-time limitations and are not expected to greatly affect the overall Z_{eff} of the plasma studied in the magnetohydrodynamic calculations in any event. In addition, processes such as forbidden radiative decays, inner-shell excitation, multiphoton processes, ion collisional excitation, cascading from higher levels, and direct double excitation were all neglected because they play a secondary role in the determination of the atomic spectra. However, the nature of the model lends itself to the addition of these processes if finer detail is required.

III. MHD SIMULATION MODEL

The ionization-dynamics model described in Sec. II was incorporated into a one-dimensional two-temperature Lagrangian MHD computer code.[15,16] The set of equations solved by the code include the two-temperature hydrodynamic equations for mass, momentum, and energy, Ohm's Law, Maxwell's equations, and an equation of state,

$$\frac{Dv}{Dt} = v\nabla\cdot\mathbf{u}, \quad (14)$$

$$\frac{Du}{Dt} = -v\nabla(p+q)+v(\mathbf{J}\times\mathbf{H}), \quad (15)$$

$$\frac{De_e}{Dt} = -vp_e\nabla\cdot\mathbf{u}+v\nabla\cdot(\kappa_e\nabla T_e)-\frac{R}{\gamma-1}\frac{(T_e-T_i)}{t_{\text{eq}}}+S, \quad (16)$$

$$\frac{De_i}{Dt} = -v(p_i+q)\nabla\cdot\mathbf{u}+v\nabla\cdot(\kappa_i\nabla T_i)+\frac{R}{\gamma-1}\frac{(T_e-T_i)}{t_{\text{eq}}}, \quad (17)$$

$$\nabla\times\mathbf{E} = -\frac{\partial\mathbf{H}}{\partial t}, \quad (18)$$

$$\nabla\times\mathbf{H} = 4\pi\mathbf{J}, \quad (19)$$

$$\eta\mathbf{J} = \mathbf{E}+\mathbf{u}\times\mathbf{H}, \quad (20)$$

$$p_\alpha v = Z_\alpha R T_\alpha, \qquad e_\alpha = \frac{Z_\alpha R}{\gamma-1}T_\alpha, \quad (21)$$

where $\alpha=e, i$, v is the specific volume, $\mathbf{u}$ is the velocity, q is the usual artificial viscosity term, κ is the thermal conductivity, t_{eq} is the equipartiation time, $\mathbf{J}$ is the current density, $\mathbf{H}$ and $\mathbf{E}$ are the magnetic and electric field intensities, p is the pressure, η is the resistivity, e is the internal energy, and Z is the charge state. The term S contains the plasma energy source and loss terms,

$$S = \Psi-\frac{\partial E_I}{\partial t}-R, \quad (22)$$

where Ψ is the Joule heating, R is the radiation emission, and dE_I/dt is the energy lost due to ionization of the plasma. The radiation-loss term contains contributions from bremsstrahlung, radiative recombination, and spontaneous decay processes. These terms are defined by[4,6]

$$R_{\text{brem}} = 1.53\times10^{-38}T_e^{1/2}n_e\sum_{z,j} z_j^2 n(z_j)\ \text{W/cm}^3, \quad (23)$$

$$R_{r-r} = 1.6\times10^{-19}n_e\sum_{zj} n(z_j)\alpha(z+1,0;z_j)\chi(z_j)\text{W/cm}^3 \quad (24)$$

$$R_{\text{line}} = 1.6\times10^{-19}\sum E_{ij}A(i,j)n(z_j)\text{W/cm}^3. \quad (25)$$

Line emission is set to zero when the ground state or Saha model is used. When the Saha equations are used to calculate ionization, an alternate form of the bound-free radiation

term is used which does not require the rate coefficient,

$$R_{r-r} = 1.53 \times 10^{-38} T_e^{-1/2} n_e \sum_{z,j} z_j^2 n(z,j) \chi(z,j) \text{ W/cm}^3. \quad (26)$$

The effective ionization Z_{eff} is calculated using Eq. (5) and inserted into the various transport coefficients. The resistivity and equipartition time (to allow for collisional transfer of energy from electrons to ions) were taken from Spitzer,[17] while Braginskii's[18] expressions were used for the ion and electron thermal conductivities.

The magnetic-diffusion and ion-temperature equations were solved implicitly while an explicit method was used for the momentum equation. A modified predictor-corrector algorithm was necessary to solve the electron-temperature equation to avoid a numerical instability caused by the ionization energy term $\partial E_I/\partial t$ in Eq. (22).

IV. NUMERICAL RESULTS

A. Validity of the ionization model

We began our studies by comparing LTE and nonequilibrium ionization models for a range of plasma temperatures and densities while ignoring (for the moment) hydrodynamic motion. In Fig. 2, we present a plot of the variation of Z_{eff} with T_e for various values of electron density n_e, as calculated by the rate-equation model (no excited states) for a helium plasma.

The steep ascents between integral values of ionization states reflect the exponential dependence of several of the rate coefficients upon electron temperature. It is this feature of these ionization calculations which can lead to an instability in the numerical methods used to solve the electron-temperature equation (16). The three different curves in Fig. 2 correspond to different ion densities, 10^{17}, 10^{18}, and 5×10^{18} cm^{-3}; the higher-density curves yield lower effective ionization. The reason for this is evident from the collisional recombination rate coefficient. Since this is a three-body collision, the number of reactions per second is proportional to n_e^2; hence, as ion and electron density increases, more collisional recombination takes place, causing lower ionization. The effect is not as marked at lower densities since radiative recombination becomes the dominant mechanism balancing collisional ionization. However, at ion densities above 10^{18} cm^{-3} in helium, for example, large deviations begin to be-

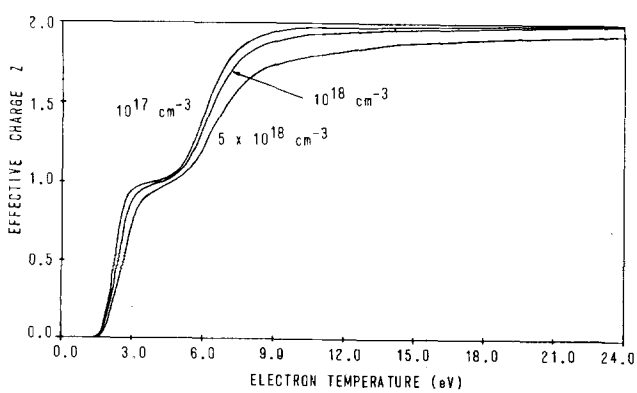

FIG. 2. Effective charge versus electron temperature for helium, calculated by the equilibrium-rate-equation model.

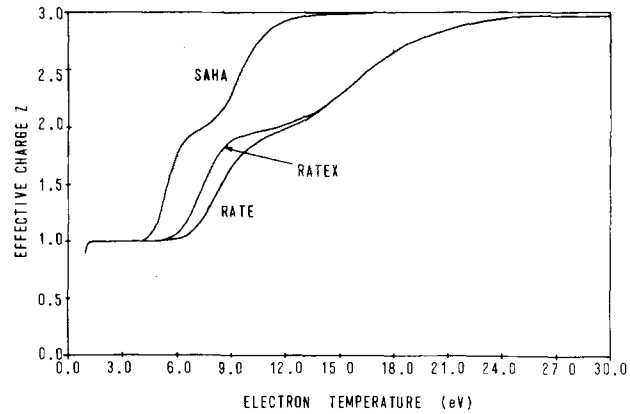

FIG. 3. Effective charge versus electron temperture for lithium at $n_i = 10^{17}$ cm^{-3}, calculated using three models.

come noticeable. One aspect of this research that should be stressed is the marginal accuracy afforded by using an LTE model to describe dense Z-pinch and exploding-wire plasmas. As electron density increases, of course, one expects a collisional-radiative rate equation model to predict values of Z_{eff} that approach the LTE model describing collision-dominated plasmas. However, the pinching and expanding hydrodynamic motion of these plasmas causes them to traverse density regimes below that at which collisional recombination dominates over radiative recombination, and the Saha equation becomes inadequate. In addition, models that are suitable for less-dense plasmas, e.g., the coronal model,[1] do not yield accurate results at dense pinch contractions. Hence, a CR model must be used to describe dense dynamic plasmas of this type. In Fig. 3, we have compared the predic-

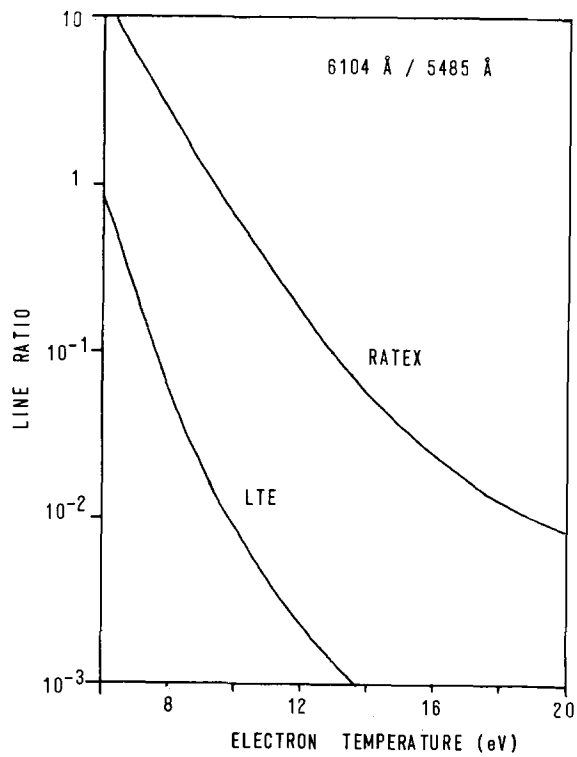

FIG. 4. Line ratio for 6104-Å/5485-Å lines of lithium at $n_i = 10^{18}$ cm^{-3}, calculated using RATEX and Saha.

tions of the Saha and CR models for the effective charge of a lithium plasma at ion densities of 10^{17} cm^{-3}. The curve labeled RATEX is for the set of rate equations including excited ion states, but neglecting the time derivative in Eq. (6), while RATE refers to the same calculation using ground-state densities only. These curves become identical at $Z_{eff} \cong 2$ since no levels of Li III were modeled. The discrepancy between the Saha and rate equations prediction becomes large as the temperature (and ionization) of the plasma increases.

The results calculated by these ionization models for the lithium plasma show interesting variations from LTE behavior in some respects. Graphs of two line rations, the 6104-Å line, $1s^2 2p(^2P)$–$1s^2 3d(^2D)$, versus the 5485-Å line, $1s2s(^3S)$–$1s2p(^3P)$, and the 6104-Å line versus the 6708-Å line, $1s^2 2s(^2S)$–$1s^2 2p(^2P)$, are shown in Figs. 4 and 5 as functions of temperature. The graphs compare an LTE calculation with that of the equilibrium CR model (RATEX) containing all the modeled excited states. The experimental data from measurements taken in our laboratory[19] on an exploding-lithium-wire plasma indicated electron temperatures of about 8–12 eV extracted from measurements of the 6104/5485 line ratio and based on an LTE calculation.[4] As seen from Fig. 4, the rate equations predict electron temperatures approximately 5–15 eV higher for a given line ratio, yielding as much as a 100% error in temperature if an LTE argument is used. However, indications are evident from Fig. 5 that LTE *is* an adequate description for the 6104/6708 line ratio. The excited levels of lithium I have evidently reached the populations given by Boltzmann equilibrium relations, while the states of lithium II have not.

Although the level structure of lithium used in this model was relatively simple, no reabsorption or transport of

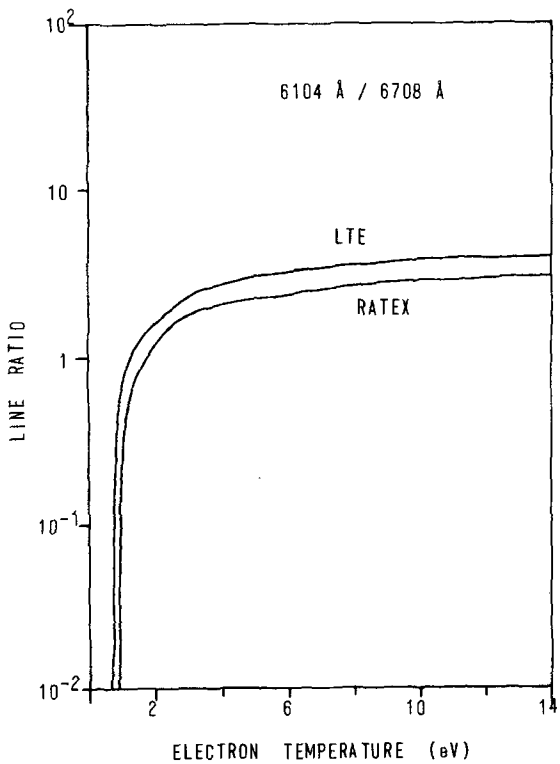

FIG. 5. Line ratio for 6104-Å/6708-Å lines of lithium at $n_i = 10^{18}$ cm^{-3}, calculated using RATEX and Saha.

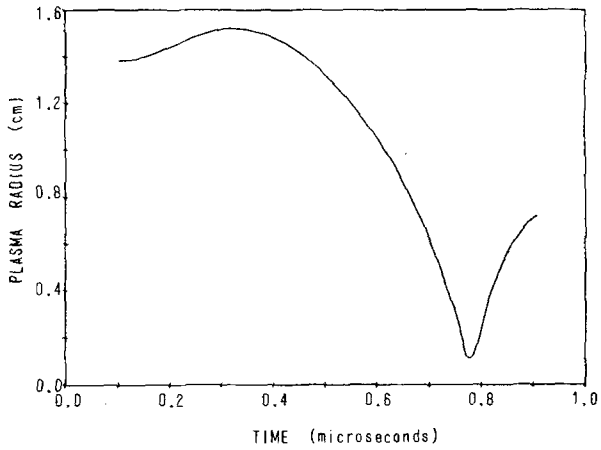

FIG. 6. Plasma radius versus time calculated by helium *Z*-pinch MHD simulation.

the radiation was included (optically thin approximation), and no spatial resolution of the lines occurring from the two different ionization stages was obtained experimentally, we feel that the theoretical calculations give strong indications of inadequacies of the LTE description for these dense low-*Z* plasmas.

B. Helium *Z*-pinch simulation studies

The main objective in simulating a dense helium *Z*-pinch plasma was to provide theoretical support for a series of experiments of this type performed in our plasma physics laboratory.[20,21] The temperature of this plasma lies in a particularly difficult range for adequate measurement and diagnostic purposes, so accurate theoretical calculations were particularly significant for the interpretation of experimental data. Moreover, the helium plasma produced in the laboratory was prepared specifically for laser interaction experiments. Hence, the simulation provided a large number of additional virtually unmeasurable plasma parameters necessary for effectively characterizing the plasma. In addition, the strong correlation between the simulation model predictions and those parameters which *could* be experimentally measured served to confirm the accuracy of the model and reaffirm its ability to generate realistic predictions corresponding to actual initial conditions.

The results presented in this section are taken from a typical simulation run, initialized to duplicate the corresponding laboratory experiment as closely as possible. The current driving the plasma dynamics was a sine wave with an amplitude of 1.4×10^5 A and a period of 8.0 μsec, although simulation runs rarely were extended beyond the first pinch time, which normally occurred at less than 0.8 μsec into the discharge. The initial plasma radius was set to 1.375 cm, and the ion plasma density was assumed to be uniform and taken to be 5.2×10^{16} cm^{-3}, defined by the fill pressure of the actual experiment and the law of mass conservation. The simulation run was begun at 0.1 μsec after initiation of the current discharge, and the ion and electron temperatures were initialized at 3.0 eV, while the effective charge was taken as 0.95 (determined by the equilibrium rate equations at these densities and temperatures). Since our present model does not describe the change of state from neutral gas to plasma,

the simulation had to be initiated at this later time with appropriate estimates of input parameters corresponding. In fact, it was found that slightly changing the input parameters T_e and Z_{eff} caused no significant effect on the plasma development.

In Fig. 6, the macroscopic fluid behavior of the plasma is shown by plotting plasma radius against time. The plasma remains at its initial radius until about 0.35 μsec, at which point the current has risen sufficiently to generate magnetic fields large enough to cause pinching contraction. The electron density, predictably enough, reaches peak values at the time of pinch which corresponds to minimum plasma radius. The particle temperatures also vary in time similar to the density, with electron temperature slightly exceeding ion temperature, since Joule heating couples with the lighter electrons more efficiently than with ions. Near the pinch, however, where shock compression becomes the dominant heating mechanism, the ion temperature exceeds that of the electrons, especially for the inner zones of the plasma (see Fig. 9). This shock heating process becomes dominant in such a short time scale that the temperature equilibration time is (relatively) too long to allow significant equipartition of this energy from ions to electrons.

Since no excited states were modeled in the helium plasma simulation, bound-bound transitions were assumed to contribute a negligible fraction of the total radiation emission. Hence, only bremsstrahlung and radiative recombination were assumed to determine the radiation energy loss. In veiw of the fact that the code predicts complete ionization during periods of maximum radiation loss (corresponding to density peaks) and spectra obtained from experiments indicate no discrete radiation above the continuum background, this assumption seems reasonable. The total radiation loss at time of pinch was calculated to be only 1.5% of the total energy addition to the plasma.

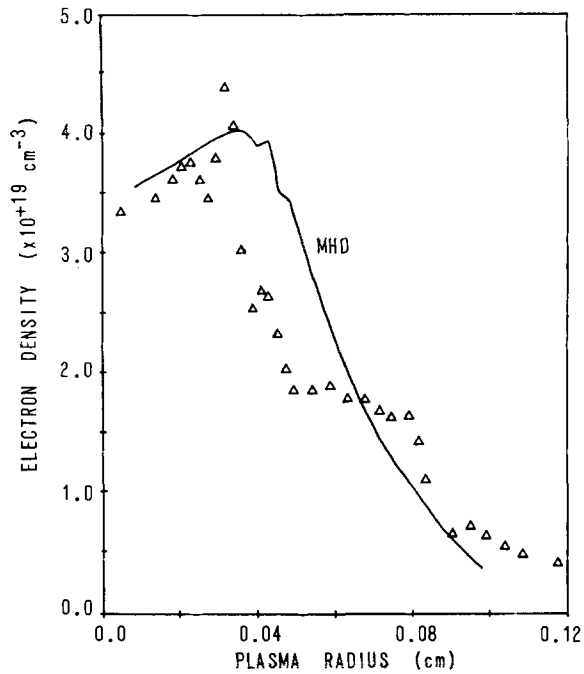

FIG. 8. Electron density versus plasma radius (at pinch time) for helium: MHD simulation and experiment.

Various parameters of interest are plotted as functions of plasma radius in Figs. 7–9. All profiles were taken at 0.76 μsec, the time of the first pinch in this run. Figure 7 shows the magneitc field profile, which drops to zero at the plasma center while rising to 1.5×10^5 G at the periphery, where the current density is the strongest. Figure 8 indicates that the electron-density profile is seen to peak, not at the plasma

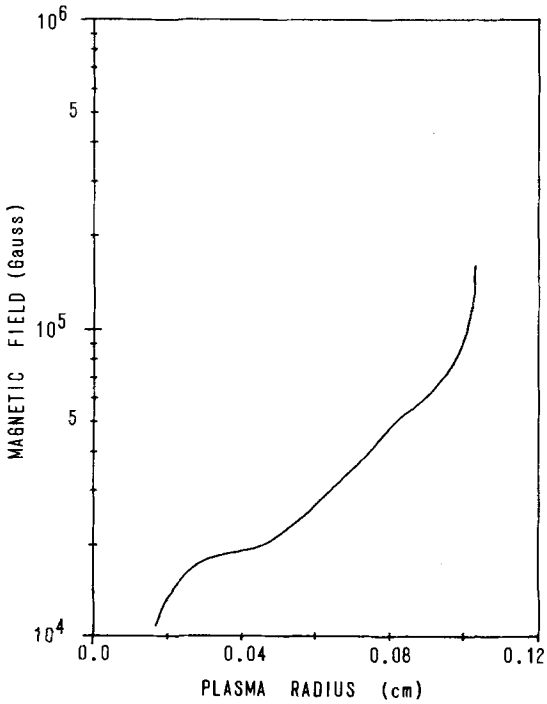

FIG. 7. Magnetic field versus plasma radius (at pinch time) calculated by helium Z-pinch MHD simulation.

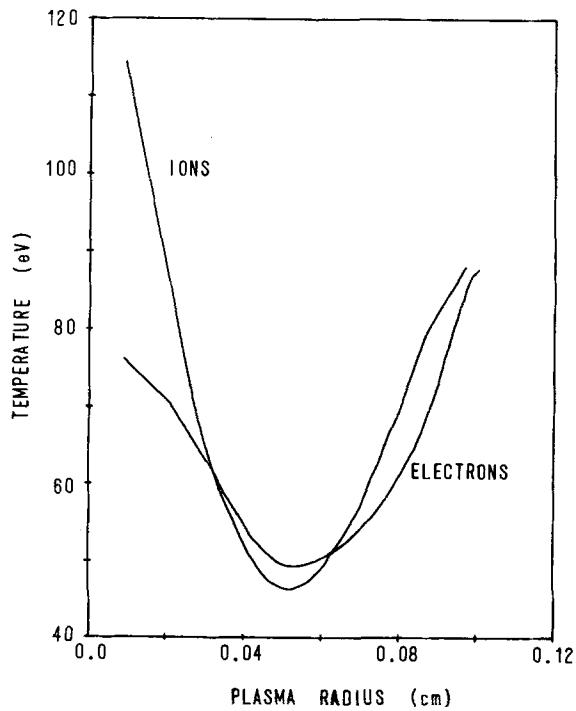

FIG. 9. Electron and ion temperatures versus plasma radius (at pinch time) calculated by helium Z-pinch MHD simulation.

center, but at a radius of approximately 0.38 mm. The density peak cannot penetrate further into the plasma because the shock heating has caused such large temperatures in the plasma interior that particle pressure drives the inner zones back outward, "squeezing" the middle zones between the pinching outer region and the expanding inner core. This temperature gradient can be seen in Fig. 9, where temperatures rise sharply near the center of the plasma. The high temperatures near the outer radius are the product of strong Joule heating of the electrons, coupled with low densities. The intermediate high-density zones are, therefore, relatively cold, as seen by the large dip in the curves.

As we noted earlier, comparison of simulation experiments involving a helium plasma with actual experiments done in our laboratory provided an excellent test of our computer model's accurcy. In particular, the electron-density profile versus radius of the plasma at time of pinch was very accurately measured in the laboratory using the techniques of interferometric holography.[22] The measurements were done with a frequency-doubled ruby laser at a wavelength of 3472 Å and pulse width of 16.0 nsec (FWHM) at 0.625 MW peak power. The data was reduced using standard Abel inversion and fitted to a curve using a spline interpolation. The ruby laser was synchronized with the plasma time evolution to produce the hologram at a time corresponding to maximum radiation emission, which was believed to be the time of the completely pinched plasma. The simulation results are plotted in Fig. 8, superimposed over the experimental data obtained from the holography. The agreement between the predicted and measured density profiles is excellent. In addition, the position and value of peak densities are in excellent agreement with experiment, corresponding to 4×10^{19} cm^{-3} at approximately the 0.36-mm radius. Also, the critical surface for CO_2 laser light, defined by the critical electron density n_c at which the laser frequency equals the plasma frequency ($n_c=10^{19}$ cm^{-3}), is calculated to occur within 1% of the measured value of 0.81 mm. The only disagreement between experiment and theory in Fig. 8 appears to be the existence of a density shelf at about 1.5×10^{19} cm^{-3}, which was not predicted by the code. Defining the electron-density scale length at the critical surface by

$$L_e=\left[\frac{1}{n_e}\left(\frac{\partial n_e}{\partial r}\right)_{n_e=n_c}\right]^{-1}\text{ cm}, \tag{27}$$

we find that this flattening causes the experimentally determined value for this parameter ($\sim80\,\mu$) to be significantly shorter than the value determined by simulation ($\sim200\,\mu$). As yet, neither modifications in our theoretical model nor further experimental measurements have been able to adequately resolve this discrepancy.

Although no other reliable accurate measurements have yet been made on the Z-pinch plasma, it is interesting to compare the temperatures at the time of the pinch which are predicted by the code with those calculated by using a very simple approximation, based upon the Bennett relation.[17] This gives the pinch current as

$$I(t)^2=\frac{N_e}{L}\,\frac{8\pi(T_e+T_i/Z)}{\mu_0}\,A^2, \tag{28}$$

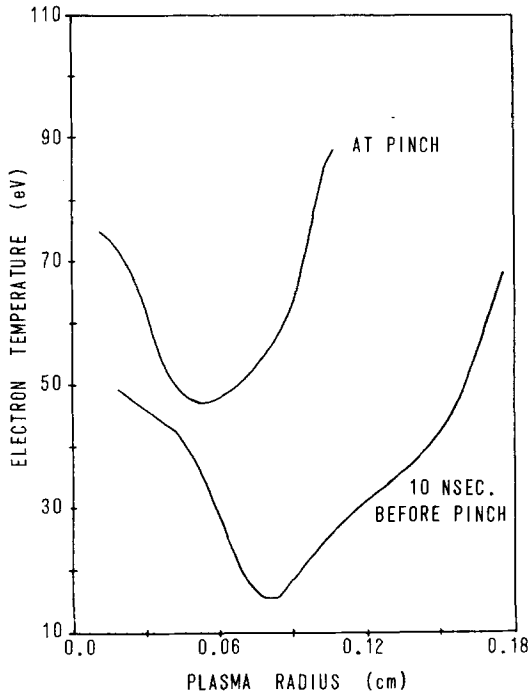

FIG. 10. Electron temperature versus plasma radius (at pinch time and 10 nsec. previous to pinch) calculated by helium Z-pinch MHD simulation.

where I is the current, L is plasma length, and N_e is total number of electrons. The electron temperature predicted by Eq. (28), using $I=8.05\times10^4$ A, $L=15$ cm, $N_e=9.65\times10^{18}$, and $Z=2$, is about 21 eV (assuming $T_e=T_i$), which is significantly different from the electron temperatures predicted by the simulation at the time of pinch, but surprisingly close to those predicted by the profile at only 10 nsec before the pinch time which is shown in Fig. 10. The dramatic rise in temperature within a 10-nsec period, as predicted by the code, is the product of strong shock heating that occurs in the central region of the plasma during this period. Such sudden rises in plasma temperature would not be predicted by the Bennett relation, since it does not take shock wave (viscous) heating into account.

V. DISCUSSION

We have attempted to demonstrate that the standard LTE treatment of dense pinched plasmas using the Saha equation is inadequate. Both the assumptions of thermodynamic equilibrium in the plasma and the neglect of radiative recombination in determining the effective plasma charge state and density distribution of ions among the various states are invalid for these plasmas. By direct comparison of theoretical calculations based upon the LTE model with those obtained from the more sophisticated model based upon time-dependent rate equations employing atomic cross-sectional data, and also by comparison of predicted line ratios with actual experimental data, we have shown that the latter model is necessary for an accurate estimate of plasma ionization dynamics.

This nonequilibrium rate-equation model has been coupled into an MHD plasma simulation and found to adequately predicted the time evolution of dense pinch plasmas.

Comparison of these predictions with experimental data supports the validity of the theoretical simulation. Such calculations have provided valuable information about these dense plasmas which will prove useful in future laser-plasma interaction experiments with intense CO_2 laser light.

[1]J. Richter, in *Plasma Diagnostics*, edited by W. Lochte-Holtgreven (North-Holland, Amsterdam, 1968).
[2]D. Bates, A. Kingston, and R. McWhirter, Proc. R. Soc. London A **267**, 297 (1962).
[3]M.J. Seaton, in *Atomic and Molecular Processes*, edited by D.R. Bates (Academic, New York, 1962).
[4]H.R. Griem, *Plasma Spectroscopy* (McGraw-Hill, New York, 1964).
[5]V. Jacobs (private communication).
[6]R.W.P. McWhirter, in *Plasma Diagnostic Techniques*, edited by R.H. Huddlestone and S.L. Leonard (Academic, New York, 1965).
[7]J. Davis and K. Whitney, J. Appl. Phys. **45**, 5294 (1974).
[8]M.J. Seaton, Phys. Soc. **79**, 1105 (1962).
[9]M.J. Seaton, Mon. Not. R. Astron. Soc. **119**, 81 (1959).
[10]W. Wiese, M. Smith, and B. Miles, *Atomic Transition Probabilities* (U.S. GPO, Washington, D.C., 1969), Vol. II.
[11]A. Burgess, Report No. AERE 4818, 1964, p. 63 (unpublished).
[12]C.W. Allen, *Astrophysical Quantities*, 2nd ed. (Athlone, London, 1955).
[13]E. Oran and J. Davis, J. Appl. Phys. **45**, 2480 (1974).
[14]J. Davis, J. Quant. Spectrosc. Radiat. TRansfer **14**, 549 (1974).
15D. Chapin, J.J. Duderstadt, and D.R. Bach, J. Appl. Phys. **45**, 1726 (1974).
[16]D. Duston, Ph.D. dissertation (The University of Michgan, 1977) (unpublished).
[17]L. Spitzer, *Physics of Fully Ionized Gases* (Interscience, New York, 1962).
[18]S.J. Braginskii, *Review of Plasma Physics* (Consultants Bureau, New York, 1965), Vol. 1.
[19]T.A. Leonard and D.R. Bach, J. Appl. Phys. **44**, 2555 (1973).
[20]P.D. Rockett, D.G. Steel, J.G. Ackenhusen, and D.R. Bach, Phys. Rev. Lett. **40**, 649 (1978).
[21]D. Duston, P. D. Rockett, D.G.Steel, J. G. Ackenhusen, D.R. Bach, and J. J. Duderstadt, Appl. Phys. Lett. **31**, 801 (1977).
[22]P.D. Rockett, Ph.D. Thesis (The University of Michgan, 1977).